Available online at www.sciencedirect.com

ScienceDirect

Energy Procedia 94 (2016) 388 – 398

Energy Procedia

13th Deep Sea Offshore Wind R&D Conference, EERA DeepWind'2016, 20-22 January 2016, Trondheim, Norway

Coherence of turbulent wind under neutral wind conditions at FINO1

Lene Eliassen[a]*, Charlotte Obhrai[b]

[a]*Norwegian Tecnhincal and Scientific University, Trondheim, Norway*
[b]*University of Stavanger, Stavanger, Norway*

Abstract

Current wind turbine design standards allow for two different approaches to model the wind field used for engineering estimates; The Mann turbulence model and the Kaimal wind spectra combined with a coherence function. The point wind spectra generated, using the recommended parameters, are similar, but there are differences in the spatial distribution of the turbulence. Especially at larger separation distances the two models will have different coherence values. As the offshore wind turbines continue to increase in rotor size, it is getting more important to model the correct spatial distribution across the large rotor areas in order to calculate the fatigue damage. There are currently few measurements of the marine boundary layer, and one of the few offshore metrological masts is located at FINO1. In this study, the measurements of the wind velocities at three different heights at FINO1 have been used to study the vertical coherence. The study is limited to January 2008, and only neutral atmospheric conditions are considered. Based on the measurements, one can see that there are large differences between the measured values and the coherence estimated by the recommended values. However, the Mann turbulence model shows a trend that is more similar to the measured coherence values, than the coherence function used with the Kaimal spectra.

Peer-review under responsibility of SINTEF Energi AS
Keywords:

1. Introduction

The offshore wind turbines are increasing in capacity [1], and thus also in rotor diameter. The aim is to harvest more energy per turbine, and reduce the levelized cost of energy (LCOE) by reducing the number of turbines in a wind farm. In order to make sure that one is actually reducing the costs, detail design of the large sized rotors should be performed. The main loading on the rotor comes from the wind, and a good description of the wind field, including turbulence intensity and spatial characteristics of turbulence, is therefore important for a good estimate of the expected fatigue loads and potential damage.

The design standard for wind turbines, IEC 61400-1, recommends both the Mann turbulence model and the Kaimal spectra in combination with the IEC coherence function to simulate the turbulent wind field. These are defined such that the turbulent wind spectrum at the hub height is similar for both turbulence models; however, there are significant differences in the spatial distribution.

The Mann turbulence model and the Kaimal model differs in how they are defined. The latter model is defined using a one-point spectra and a coherence function, while the Mann turbulence model is defined using spectral velocity tensors. Both methods contain the same amount of information, but the Mann turbulence model includes a more natural and direct representation of the three

* Corresponding author. Tel.: +0-000-000-0000 ; fax: +0-000-000-0000 .
E-mail address: lene.eliassen@ntnu.no

Peer-review under responsibility of SINTEF Energi AS
doi:10.1016/j.egypro.2016.09.199

dimensional turbulent flow [2]. The Mann model is based on an application of rapid distortion theory, which implies a linearization of the Navier-Stokes equations [3].

The spatial statistics of inflow turbulence was examined as a part of the Long-term Inflow and Structural Test (LIST) program. In [4] the coherence for the three turbulence components was estimated and compared to the coherence functions available in the literature. These measurements were from an onshore site, and the separation distances were relatively small. For offshore wind conditions, there are few studies investigating the spatial distribution in the wind. The main reason is the large cost involved in conducting offshore wind measurements.

There are a few metrological masts installed offshore and one of these is the FINO1 research platform, located 45 km to the north of the German island of Borkum in a water depth of approximately 30 m [5]. The wind measuring mast is 80 m, and with the platform being located 23 m above LAT (low atmospheric tide), the top of the mast is at an altitude of max 103 m. The mast is equipped with ultrasonic anemometers, wind vanes, cup anemometers and temperature measurements. In addition to these measurements, there are also wave buoys that are used to measure wave height, period and direction close to the research platform [6] [7].

The aim of this study is to investigate the spatial distribution of the wind at the FINO1 platform under neutral atmospheric conditions. This study has here been limited to the month of January 2008, which had the highest occurrence of neutral conditions for the time period investigated.

2. Method

In order to compare the spatial distribution in the measured wind field to the ones given in the standard, the parameter of co-coherence will be used in this study. The co-coherence is the real part of the cross-spectral energy of the wind velocities at two different heights divided by the autospectrum function:

$$co-coherence = \frac{real(S_{xy})}{\sqrt{S_x S_y}} \tag{1}$$

The co-coherence was estimated using a set of 10-min time series data, which needed to be first checked for stationarity and then for the state of neutral atmospheric stability. It was also necessary to ensure that the measurements were within the surface layer, and that the metrological mast was not distorting the incoming wind field. The methods for doing this are presented in the following section and are followed by the co-coherence functions given in the IEC 61400-1.

2.1. FINO1 measurement data

The metrological mast on the FINO1 research platform is equipped with three Gill R3-50 ultrasonic anemometers [8] at 40 m, 60 m and 80 m that will be used to measure the co-coherence at three vertical separations. The wind measurements are in the mast shadow when the incoming wind direction is from north-west. Therefore, all wind directions from 90degs to 160degs were excluded from the analysis. Fig 1 shows the distribution of records in each 1ms^{-1} velocity bin used in the analysis. These records represent all the conditions during January 2008 that were not in the mast shadow, that were stationary and with neutral atmospheric stability

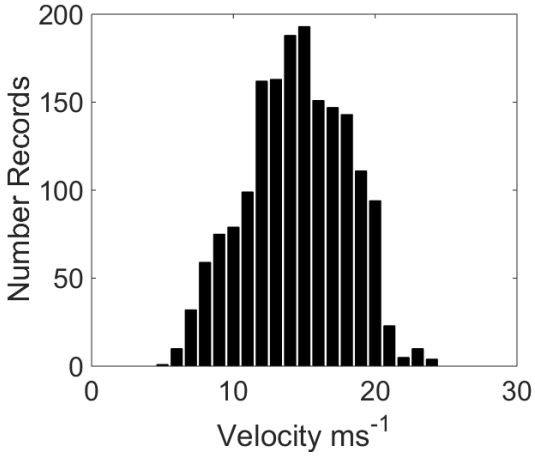

Fig. 1. Number of records per wind velocity bin.

Atmospheric stability was measured using the velocity and temperature measurements at 40m and 80m to calculate the gradient Richardson number.

$$Ri = \frac{g(\Delta\theta/\Delta z)}{\overline{T}(\Delta u/\Delta z)^2}$$

where θ is the potential temperature and T is the mean temperature. The conditions were then classified as neutral conditions, when the gradient Richardson number was between -0.569 and 0.083 [9].

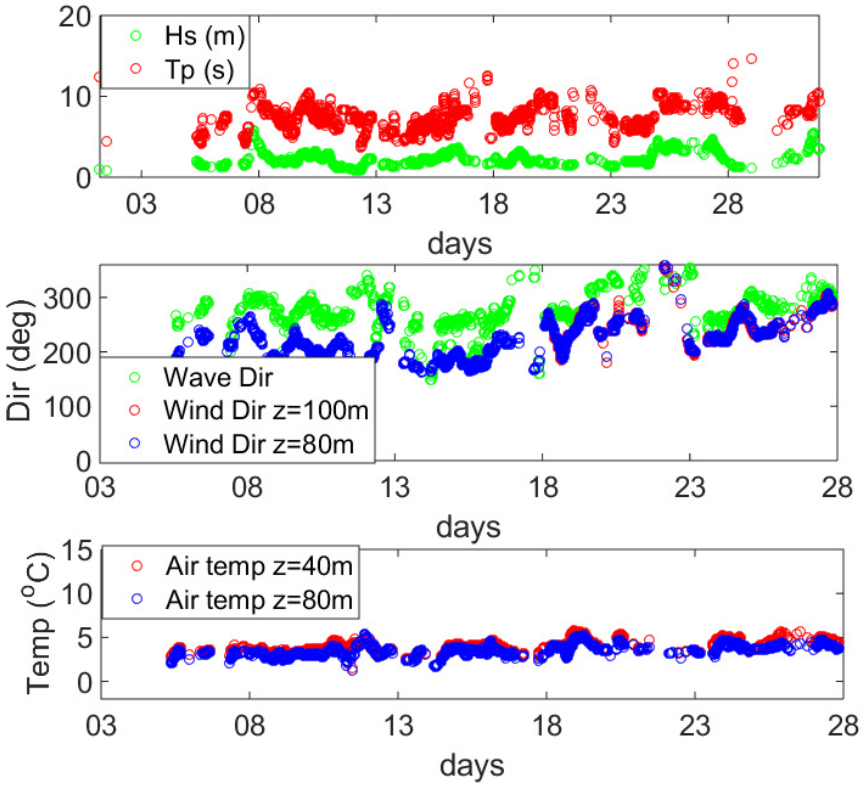

Fig. 2. The 10 min average data set used for the presented investigation. Only selected data points are shown. The top graph shows the wave buoy measurements, the middle graph the wave direction (green) and wind directions (red @ z=100 m, blue @ z=80 m) and the bottom graph presents the air temperature at 40 m (red) and at 80 m (blue).

The 10 min average data sets of the wave buoy movement, wind and wave directions and the temperature at 40 m and 80 m heights of all samples included in the study are shown in Fig. 2. In the top graph the wave buoy motion describes the roughness of the sea at the different 10-min samples and the middle graph illustrates that the wind directions measured at 80 m and 100 m are similar. The wind directions are in blue and in red, while the green dots are the wave directions and most of the time the wind and waves are misaligned. The bottom graph is the air temperature 40 m and 80 m. Most of the time the temperature is higher at 40 m compared to 80 m, which indicates a slightly unstable atmospheric condition.

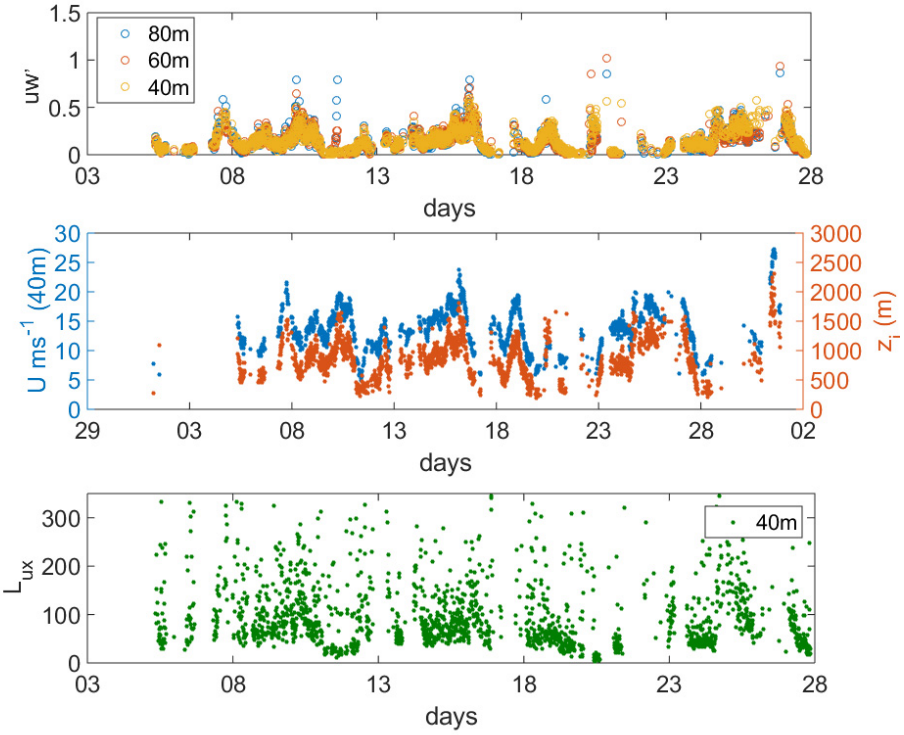

Fig. 3. The 10 min average data set. Only selected data points are shown. Top graph presents the turbulent momentum flux (u'w') measurements at three different heights (blue @ 80 m, red @ 60 m and yellow @ 40 m), middle graph is showing the boundary layer height (red) and the mean wind velocity (blue) and the bottom graph is the integral length scale.

In Fig. 3 the top graph shows the turbulent momentum flux (u'w') values. These are estimated at three different heights, and for most of the cases they are similar at the three altitudes. This is an indication that the measurements are done within the surface layer. In the middle graph, an estimate of the surface layer height, z_i, is shown in red. In the same graph the mean wind speed at 80 m height is shown in blue. It is seen that there was strong winds for many of the measurements. The bottom graph is showing the variation of the integral length scale, L_{ux}.

2.2. Turbulence models

There are two turbulence models given in the IEC 61400-1 [10], the Kaimal spectrum combined with the IEC coherence model and the Mann uniform shear turbulence model. These are referred to as the Kaimal model and the Mann model in this study. The Kaimal model is defined with a point spectrum and a coherence function. The IEC coherence function is defined as:

$$coherence = \exp\left[-12\left(\left(f \cdot r / V_{hub}\right)^2 + \left(0.12r / L_C\right)^2\right)^{0.5}\right] \quad (1)$$

If the separation is kept constant, there will still be a variation in the coherence due to velocity changes. However, when using the reduced frequency, $f_r = f \cdot r/V_{hub}$, to visualize the coherence, the coherence at all wind speeds with equal separation distance, will follow the same curve.

The co-coherence function of the Mann model is more complex to find, since the Mann model is based on a velocity spectral tensor. The spectral tensor components are listed in the Appendix A. Based on the velocity spectral tensor one can compute the coherence as:

$$co-coherence = \frac{real(\int_{-\infty-\infty}^{+\infty+\infty}\int \phi_{ij}(k_1,k_2,k_3)\exp(-ik_2\delta_2)\exp(-ik_3\delta_3)dk_2dk_3)}{\sqrt{\int_{-\infty-\infty}^{+\infty+\infty}\int \phi_{ii}(k_1,k_2,k_3)dk_2dk_3 \int_{-\infty-\infty}^{+\infty+\infty}\int \phi_{jj}(k_1,k_2,k_3)dk_2dk_3}} \quad (1)$$

where i and j=1,2,3 for the along-wind, the across-wind and vertical turbulence components, respectively, δ_2, δ_3 are the nondimensionalised spatial separation vector components, defined as $\delta_i = D_i/l$, k_1, k_2, k_3 are the nondimensional spatial wave numbers, defined as $k_i = 2\pi f l/V$, l is an isotropic scale parameter proportional to the isotropic integral length scale L.

3. Results

3.1. Co-coherence in velocity bins

The co-coherence was estimated based on the wind velocity components from the sonic anemometers at 40 m, 60 m and 80 m. Consequently one can study the co-coherence at two different separation distances; 20 m and 40 m. The 20 m separation distance can be studied both between 40 m and 60 m and between 60 m and 80 m. Only the co-coherences measured between the sonics located at 40 m and 60 m is shown below, however the trend is similar for the other measurements as shown later, in Fig. 7.

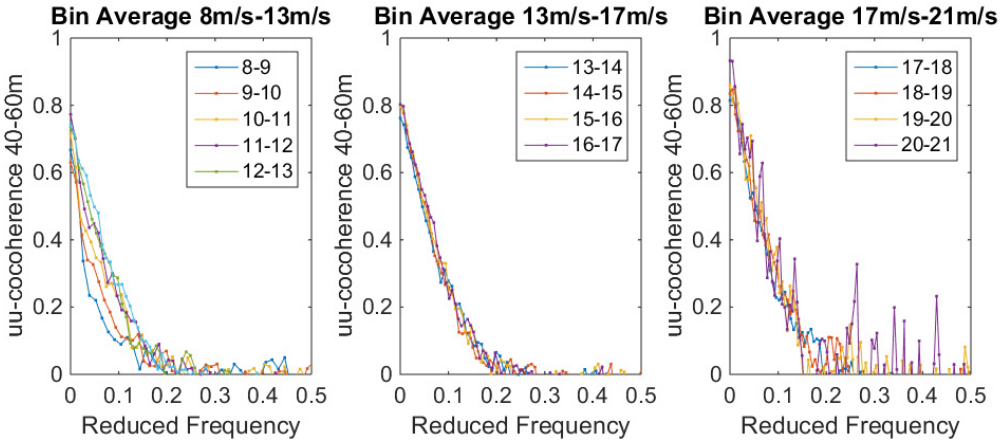

Fig. 4. The results for the co-coherence of the along-wind velocity component (u) measured at 40 m and 60 m. The results are separated into bins according to the mean wind speed in the along-wind direction.

In Fig. 4 the co-coherence of the along-wind component (u) is shown. It was found that the lower wind velocities behaved differently to the higher wind velocities, and it was therefore chosen to separate them according to their mean wind velocities. The reduced frequency is used along the x-axis, and as expected the lines in each graph follow similar trends independent of the mean wind velocity for higher wind speeds. However, it should also be noted that at lower wind speeds, the amplitude of the uu-co-coherence is lower compared to the higher wind speeds.

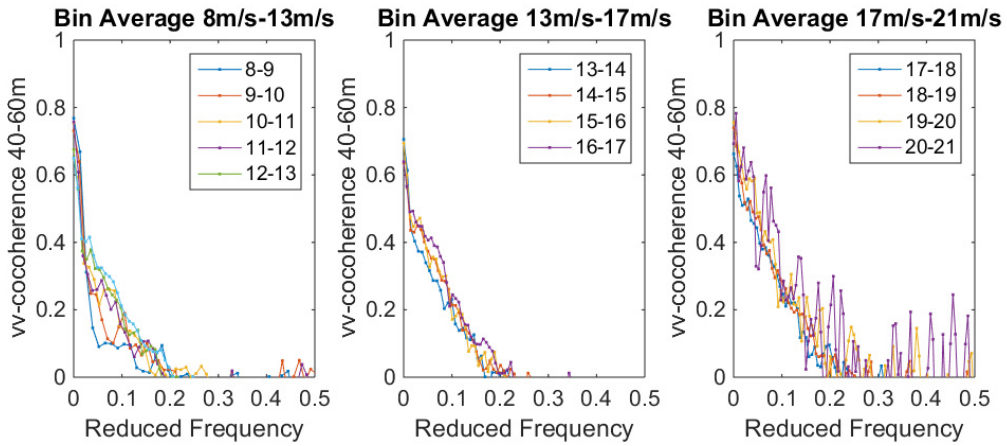

Fig. 5. The results for the co-coherence of the cross-wind velocity component (v) measured at 40 m and 60 m. The results are separated into bins according to the mean wind speed in the along-wind direction.

In Fig. 5 the co-coherence for the cross-wind component (v) is shown. Similar to the along-wind component, the results have been separated into low wind speed, middle wind speed and high wind speed. There seems to be no large differences between the wind velocities in amplitude, but the decay rate of the vv-co-coherence is larger for the smaller wind speeds.

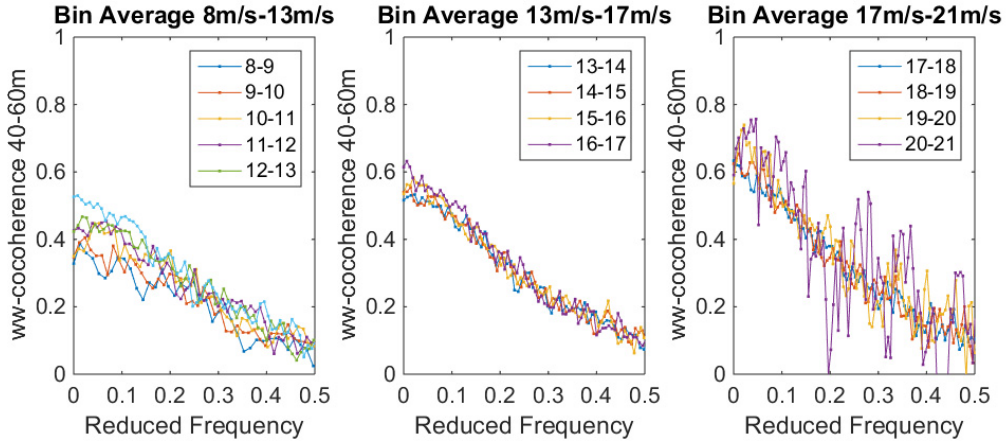

Fig. 6. The results for the co-coherence of the vertical velocity component (w) measured at 40 m and 60 m. The results are separated into bins according to the mean wind speed in the along-wind direction.

The last co-coherence component is the vertical wind component (w) shown in Fig. 6. Both the amplitude and the decay rate are lower for the vertical wind component, compared to both the along-wind and cross-wind components. There is also a clear difference between the amplitude of the co-coherence of the vertical wind speed w at low wind speeds compared to higher wind speeds.

3.2. Co-coherence at 20 m and 40 m separations

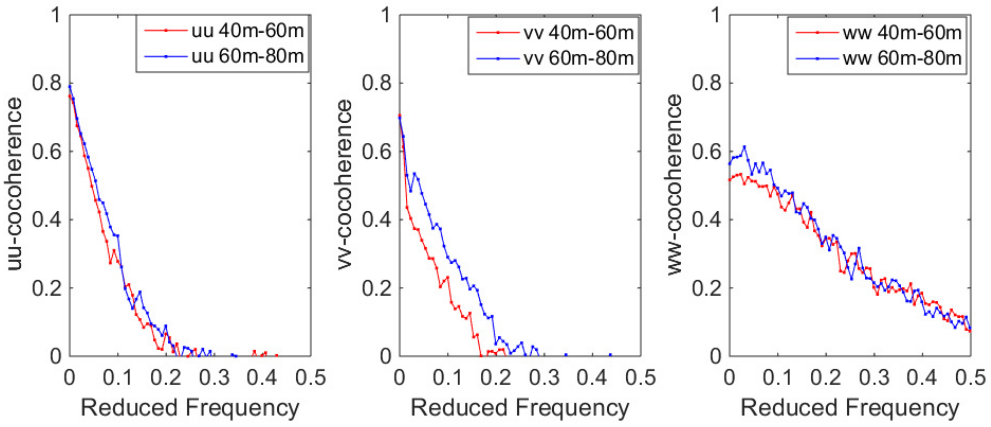

Fig. 7. The results for the co-coherence of the three velocity components measured at a 20m separation. The measurements at 40 m and 60 m are in red and measurements at 60 m and 80 m are in blue.

The co-coherence was estimated for 20 m separation for heights at 40 m and 60 m, and also at 60 m and 80 m. The average co-coherence for all wind speeds are compared for the two 20m separations where the left graph shows the along-wind component, the middle is the cross-wind and the right graph is the down-wind component. The two sets of measurements are very similar, and this indicates that the co-coherence of the along wind velocity is not varying with height under neutral wind conditions.

For measurements close to the ground, one may expect that the distance to the ground may effect the co-coherence. Since the differences between the co-coherences are small for the two heights, these grounds effects are assumed negligible at heights above 40 m.

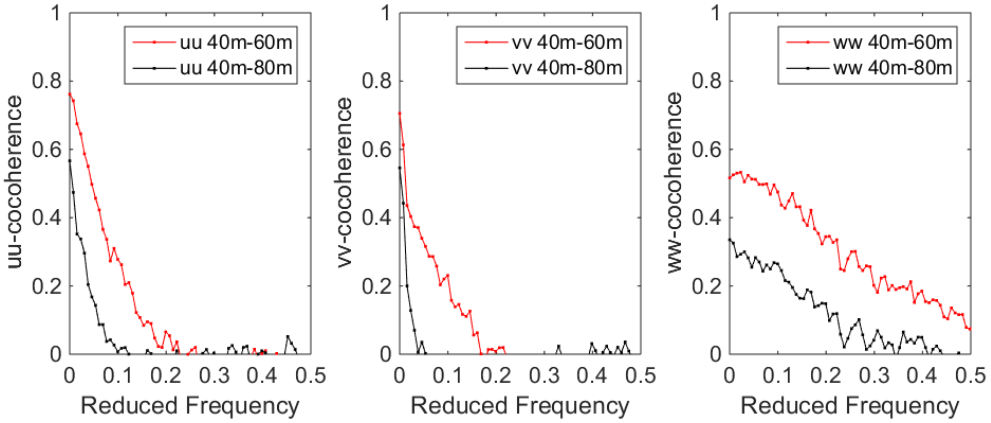

Fig. 8. The results for the co-coherence of the three velocity components measured at 20 m (red) and 40 m (black) separation distance.

Fig. 8 shows the co-coherence for 20 m separation (red) and the 40 m separation (black). As expected, the larger vertical separation of 40m has a lower co-coherence than the smaller vertical separation of 20m for all wind components.

4. Discussion

For wind turbine loading, it is the along-wind component that is the most important of the three velocity components. Therefore, one of the turbulence models in the IEC 61400-1, the Kaimal model, only considers the coherence of the turbulence in the along-wind direction.

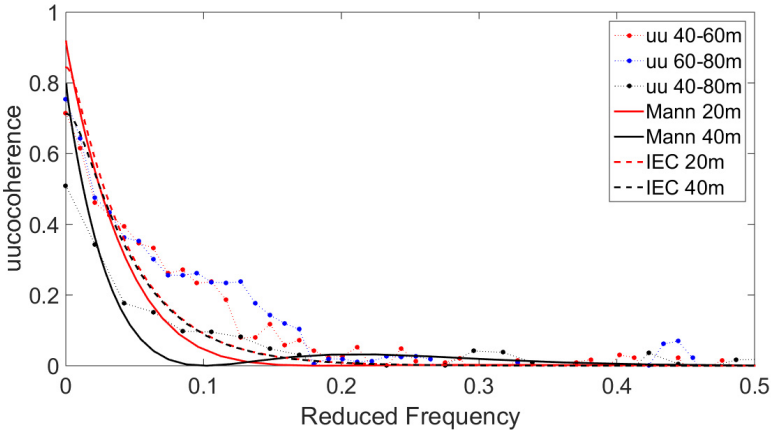

Fig. 9. Comparing the co-coherence of the along-wind component at 40 m (black) and 60 m (red) separation distance. Measurements are marked as dots, the IEC coherence function is a dashed line, and the Mann turbulence model is shown as a solid line.

A comparison between the co-coherence of the along-wind component for the two turbulence models and the measured values from the FINO1 mast is shown in Fig. 9. For the lower separation, 20 m (red), both turbulence models underestimate the co-coherence of the along wind velocity component, while at the larger separation, 40 m (black), the IEC coherence function is above the measured values and the Mann model is very close to the measured values.

In Fig. 9, it is can be seen that the difference in co-coherence for the IEC coherence function at different separations is limited to the lower reduced frequencies (<0.05Hz). However, both the measurements and the Mann model show significant differences in the co-coherence over a larger range of reduced frequencies (<0.15Hz).

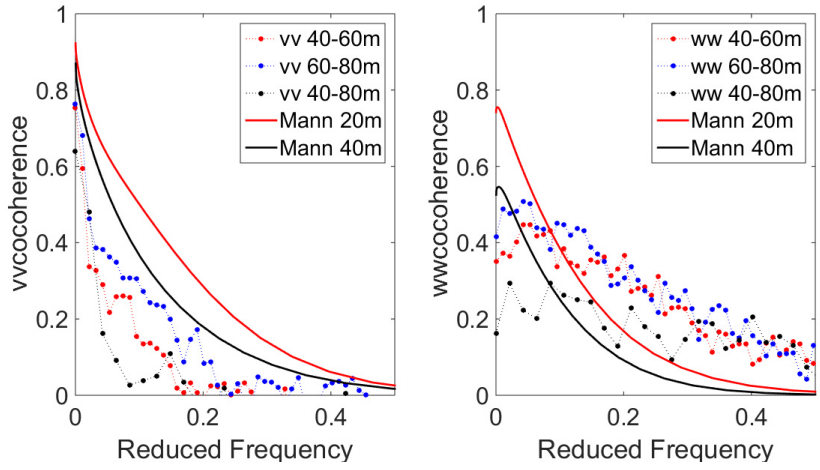

Fig. 10. Comparison of the co-coherence of the cross-wind (left) and vertical wind component (right) at 40 m (black) and 60 m (red) separation distance. Measurements are marked as dots, and the Mann turbulence model is shown as a solid line.

The IEC coherence function is not included in the comparison between the co-coherence of the cross-wind and down-wind components in Fig. 10, since this function is only valid for the along-wind component. Figure 10 shows that the measured co-coherences of the cross-wind component v are lower than what is estimated by the Mann turbulence model for both separation distances. The measured co-coherence of the vertical wind component w compares well to the Mann turbulence model for the 40 m separation distance. For the 20 m separation, the Mann model is however lower than the measured values, which is similar to the comparison of the co-coherence in the along-wind direction.

4. Conclusion

Our motivation for comparing the measured spatial turbulent structure to the turbulence model in the IEC 61400-1 is that it will influence the design loads for offshore wind turbines. The turbulence models are used to simulate the wind fields used in design load calculations, and the spatial distribution of the turbulence will influence the response. It was shown by Eliassen et al [11] that an increase in coherence will result in an increase in fatigue loads.

The IEC coherence model shows small variances for different separation distances relative to the reduced frequency. Only at the lower values of the reduced frequency was there a small decrease in the co-coherence. However, the measurements indicate that there are larger differences for the two vertical separations (20m & 40m) for reduced frequencies of up to 0.15Hz which is not represented by the IEC coherence function. For separations than larger 40m, one can therefore evaluate a higher coherence in the wind field when using the IEC coherence function. Consequently the estimated loads from the simulation will be overestimated.

However, for the Mann turbulence model, one can see a larger difference for the two separations, similar to the measurements. The best fit is found for the 40 m separation, especially for the along-wind and vertical wind components. No work has been done to try to fit the Mann model to the specific site data, and the parameter values used in the study are the same as recommended by the IEC 61400-1.

In future, more data will be studied, and more stability classes will be evaluated. In addition, one will try to make a better fit of the Mann model by adjusting the parameters used. There are also parallel studies ongoing quantifying the difference in fatigue damage due to the two different turbulence models.

Acknowledgements

The FINO1 platform is one of three offshore platforms of the FINO Project [5], funded by the Federal Ministry for the Environment, Nature Conservation and Nuclear Safety (BMU).

The work was partly carried out in the DIMSELO project, which is a Knowledge-building Project for Industry funded by the Norwegian Research Council (NRC) under the ENERGIX program. The project is also funded by its industry partners Statoil and Statkraft. The projects research organization partners are IFE, NTNU and DTU.

The work has partly been funded by NORCOWE, which is a consortium with partners from industry and science.

Appendix A.

A.1. The Mann turbulence model

The Mann model differs from the Kaimal spectral and exponential coherence model in that a three dimensional velocity field is defined. The isotropic von Karman energy spectrum [12] is used, and it is assumed that it is distorted by a uniform mean velocity shear. The velocity spectral tensors are given as [7]:

$$
\begin{aligned}
\phi_{11}(k_1,k_2,k_3) &= \frac{E(k_0)}{4\pi k_0^4}(k_0^2 - k_1^2 - 2k_1(k_3+\beta(k)k_1)\zeta_1 + (k_1^2+k_2^2)\zeta_1^2)\\
\phi_{22}(k_1,k_2,k_3) &= \frac{E(k_0)}{4\pi k_0^4}(k_0^2 - k_2^2 - 2k_2(k_3+\beta(k)k_1)\zeta_2 + (k_1^2+k_2^2)\zeta_2^2)\\
\phi_{33}(k_1,k_2,k_3) &= \frac{E(k_0)}{4\pi k^4}(k_1^2+k_2^2)\\
\phi_{12}(k_1,k_2,k_3) &= \frac{E(k_0)}{4\pi k_0^4}(-k_1k_2 - k_1(k_3+\beta(k)k_1)\zeta_2 - k_2(k_3+\beta(k)k_1)\zeta_1 + (k_1^2+k_2^2)\zeta_1\zeta_2)\\
\phi_{13}(k_1,k_2,k_3) &= \frac{E(k_0)}{4\pi k_0^2k^2}(-k_1(k_3+\beta(k)k_1) + (k_1^2+k_2^2)\zeta_1)\\
\phi_{23}(k_1,k_2,k_3) &= \frac{E(k_0)}{4\pi k_0^2k^2}(-k_2(k_3+\beta(k)k_1) + (k_1^2+k_2^2)\zeta_2)
\end{aligned}
\tag{1}
$$

where *i* and *j*=1,2,3 for the along-wind, the across-wind and vertical turbulence components, respectively and k_1, k_2, k_3 are the nondimensional spatial wave numbers for the three component directions, defined as $k_i = 2\pi f l/V$, l is an isotropic scale parameter proportional to the isotropic integral length scale *L*, *k* is the magnitude of the non-dimensional wave vector:

$$k = \sqrt{k_1^2 + k_2^2 + k_3^2} \tag{1}$$

k_0 is the magnitude before shear distortion:

$$k_0 = \sqrt{k^2 + 2\beta(k)k_1k_3 + (\beta(k)k_1)^2} \tag{1}$$

$\beta(k)$ is a non-dimensional distortion time:

$$\beta(k) = \frac{\Gamma}{k^{2/3}\sqrt{{}_2F_1(\frac{1}{3}, \frac{17}{6}, \frac{4}{3}, -k^{-2})}} \tag{1}$$

where ${}_2F_1$ is the hypergeometric function, Γ is a non-dimensional shear distortion parameter and *E(k)* is the non-dimensional, von Karman isotropic energy spectrum

$$E(k) = \frac{1.453k^4}{(1+k^2)^{17/6}} \tag{1}$$

where ζ_1 and ζ_2 are variables defined as:

$$\zeta_1 = C_1 - \frac{k_1}{k_2}C_2, \quad \zeta_2 = \frac{k_2}{k_1}C_1 + C_2 \tag{1}$$

where C_1 and C_2 are:

$$C_1 = \frac{\beta(k)k_1^2(k_1^2 + k_2^2 - k_3(k_3 + \beta(k)k_1))}{k^2(k_1^2 + k_2^2)},$$
$$C_2 = \frac{k_2^2k_0^2}{(k_1^2 + k_2^2)^{3/2}}\arctan\left(\frac{}{k_0^2(k_3 + \beta(k)k_1)k_1\beta(k)}\right) \tag{1}$$

References

[1] E.W.E. Association, The European offshore wind industry - key trends and statistics 2015, in: I. Pineda (Ed.), 2016.
[2] J. Mann, Wind field simulation, Probabilistic engineering mechanics, 13 269-282.
[3] J. Mann, The spatial structure of neutral atmospheric surface-layer turbulence, Journal of Fluid Mechanics, 273 (1994) 141-168.
[4] K. Saranyansoontorn, L. Manuel, P.S. Veers, A comparison of standard coherence models of inflow turbulence with estimates from field measurements, Journal of Solar Engineering, 126 (2004) 1069-1082.
[5] F.-u. Entwicklungszentrum, FINO1 - Forschungsplattformen in Nord- und Ostsee Nr.1, in, www.fino1.de, visited on 02.02.2016.
[6] Argyriadis, K., G. Fischer, P. Frohböse, D. Kindler, F. Reher, Research platform FINO1 – some measurement results, EWEC, Business, Science and Technology, Athens, 2006.
[7] Beeken, A., T. Neumann, and A. Westerhellweg, Five years of operation of the first offshore wind research platform in the

German Bight – FINO1, DEWEK 2008, Bremen (http://www.fino1.de/forschungsdaten/ergebnisse)
[8] Gill Instruments Limited: *"R3-50 Ultrasonic Research Anemometer"*, Datasheet, 2001
[9] C. Obhrai, S. Kalvig, O.T. Gudmestad, A review of current guidelines and research on wind modelling for the design of offshore wind turbines, in: Twenty-second (2012) International Offshore and Polar Engineering Conference, Rhodes, Greece, 2012.
[10] I.E.C. (IEC), IEC 61400-1 Wind turbines - Part 1: Design requirements, in, 2007.
[11] L. Eliassen, J. Jakobsen, J. Krokstad, The effect of turbulent wind field on loads of a wind turbine rotor of increasing size, in: 14th International Conference on Wind Engineering, Porto Alegre, Brazil, 2015.
[12] T.v. Kármán, Progress in the statistical theory of turbulence, Proceedings Nat. Acad. Sci., 34 (1948).